Engineering Structures 238 (2021) 112200

Contents lists available at ScienceDirect

Engineering Structures

journal homepage: www.elsevier.com/locate/engstruct

Quasi-plastic flexural behavior of adhesive-bolt hybrid connection for large scale pultruded GFRP frame

Peng Feng [a,*], Yuwei Wu [a], Yi Ding [b], TianQiao Liu [a], Ye Tian [c]

[a] Department of Civil Engineering, Tsinghua University, Beijing 100084, China
[b] Central Research Institute of Building and Construction, MCC Group, Beijing 100088, China
[c] China Architecture Design and Research Group, Beijing 100084, China

ARTICLE INFO

Keywords:
Pultruded GFRP composite material
Adhesive-bolt hybrid connection
Quasi-plastic flexural behavior

ABSTRACT

Flexural behavior of an adhesive-bolt hybrid connection for pultruded glass fiber reinforced polymer (GFRP) frame is investigated through monotonic and cyclic loading tests. It is shown that the hybrid connection fabricated using resin adhesive and steel bolts is able to exhibit a quasi-plastic behavior. Multistage damage occurred in tests, and the adhesive failed initially, followed by GFRP failure at bolt holes. Effect of shear force was investigated by variable shear-span ratios in tests. Additionally, moment and rotation curves obtained from monotonic and cyclic loading tests are found to be similar, indicating that loading schemes have little impact on structural performance of the hybrid connection. Energy dissipation is analyzed based on cyclic loading tests. Finite element model is also built, and design formulas are proposed to predict the quasi-yield moment and maximum moment. A good agreement is found between experimental results and analytical predictions. In addition, design recommendation on the use of adhesive-bolt hybrid connection is provided.

1. Introduction

In the past decades, pultruded glass fiber reinforced polymer (GFRP) composites are increasingly used in civil infrastructures. With the continuous improvements of the pultrusion process as well as the developments of the design guides, applications of all-GFRP structures have seen a considerable increase worldwide. Due to the high strength-to-weight ratio, and superior resistance to fatigue and corrosion, all-GFRP composite structures, in many scenarios, are found to be excellent alternatives to those structures built using conventional construction materials[1–4]. In particular, connections in GFRP structures are deemed to be essential in providing the required load-carrying capacities. Due to the significant impact of the stress concentration and initial defect [5], premature failure of the connections may lead to catastrophic failure of the entire structure, while the load-carrying capacity of GFRP members may not be fully used, resulting in the inefficient use of material. In this regard, sufficient strength of connections serves as the basis in achieving the expected structural behaviors of GFRP profiles. The adhesive-bolt hybrid connections have been applied in some structures, and exhibited a great mechanical performance [6,7]. Efforts from many researchers have been made to address the structural behavior as well as the design method of the connections in GFRP structures [8–11].

Bank et al. proposed four connection designs based on the failure mode of GFRP structures observed in tests [12]. It was found that the connection having gusset plate and stiffeners provided the best structural performance, showing a linear elastic relationship between moment and rotation; while the other three connections, made by GFRP angle-sections and steel bolts, were found to have lower moment resistance and rotational stiffness, and showed a nonlinear moment and rotation response. Although Bank et al. recommended using adhesive and mechanical fasteners in connections, performance of the adhesive was not quantitively addressed in their work. Later, Bank et al. continued their previous work and proposed four more connection designs [13]. Connection having a wrapped angle was found to have the best performance. In addition, in this connection, adhesive, mechanical fasteners and tubular stiffeners were used.

Smith et al. conducted an experimental test to study the behavior of connections for pultruded GFRP I- and box-sections [14]. It is found that box-section connections performed much better than the I-section connections in terms of both strength and stiffness. Carrion et al. [15], Singamsethi et al. [16] and Qiu et al. [17] also carried out experimental studies on cuff connections that were specifically used for GFRP box- and circular-sections. These new connections were fabricated using a

* Corresponding author.
E-mail addresses: fengpeng@tsinghua.edu.cn (P. Feng), wyw16@mails.tsinghua.edu.cn (Y. Wu), liu_tianqiao@mail.tsinghua.edu.cn (T. Liu), tiany@cadg.cn (Y. Tian).

https://doi.org/10.1016/j.engstruct.2021.112200
Received 6 October 2020; Received in revised form 3 March 2021; Accepted 5 March 2021
Available online 1 April 2021

Nomenclatures

a	lever arm length
b	section width
D	generalized deformation to determine the damping ratio
D_{max}	maximum generalized deformation to determine the damping ratio
d_i	diameter of the bolt
E_L^t	longitudinal tensile modulus
E_T^t	transverse tensile modulus
E_L^c	longitudinal compressive modulus
E_T^c	transverse compressive modulus
E_D	dissipated energy by damping
E_{SO}	dissipated energy by nonlinear behavior
F	generalized force to determine the damping ratio
F_{max}	maximum generalized force to determine the damping ratio
F_L	longitudinal strength
f_L^t	longitudinal tensile strength
f_T^t	transverse tensile strength
f_L^c	longitudinal compressive strength
f_T^c	transverse compressive strength
$f_{c,L}$	longitudinal bolt hole bearing strength of the GFRP sections
$f_{c,T}$	transverse bolt hole bearing strength of the GFRP sections
f_v^b	shear strength of bolts
G_m	shear modulus of adhesive
h	section height
I	moment of inertia of the member about the axis of bending
$K_{\theta,e}$	rotation stiffness in elastic stage
M_b	theoretical bending capacity of the beam profile
M_{exp}	experimentally determined moment capacities
M_f	final moment resistance when tests ended
M_{FEM}	moment capacities determined by FEM model
M_m	maximum moment resistance
M_{pred}	moment capacities determined by design equation
M_u	0.85 times of maximum moment resistance
M_y	quasi-yield moment
n	number of bolts
n_v	number of shear interface in bolts
P_y	quasi-yield load
r	distance between the corner of the adhesive zone and the rotational center
r_i	distance between the rotational center and the bolt
t	GFRP section thickness
$V_{br,i}$	pin-bearing strength of the ith bolt
$V_{bt,i}$	bolt shear strength of the ith bolt
$V_{u,i}$	shear resistance of the ith bolt
y	distance from the neutral axis to the extreme fiber of the member
α	the angle between stress at bolt and pultrusion direction
θ_f	final rotation at final moment resistance
θ_m	peak rotation at maximum moment resistance
θ_u	ultimate rotation corresponding to 0.85 M_m
θ_y	quasi-yield rotation
ζ	equivalent viscous damping ratio
λ	shear-span ratio
η	dimensionless parameter of connection effectiveness
μ_θ	ductility factor
ν	major Poisson's ratio
τ_m	shear strength of the adhesive

vacuum assisted resin transfer molding (VARTM) process. Failure modes, including bond failure, cuff failure and beam crashing, were studied. Qureshi and Mottram tested beam-to-column connections having FRP and steel cleats [18]. It was found that when FRP cleats were used, connection failure typically occurred at FRP cleats by delamination cracking at the top of cleats; and when steel cleats were used, connection failure shifted from the FRP cleats to the column, indicating a higher connection strength.

From previous studies, it is shown that the hybrid connection, a combination of adhesive bonding and mechanical fastening, has a higher static and fatigue strength when compared to rivet or bonded connections [19–22]. When using hybrid connection in GFRP structures, the connection is able to provide a higher stiffness and behaves in a quasi-plastic pattern [23–25].

Typically, a hybrid connection shows a multistage structural behavior [21,23–25]. For example, Kelly studied the quasi-static strength and fatigue performance of a hybrid connection. In the fatigue life, three stages were observed, as shown in Fig. 1 [21]. In the first stage, adhesive alone provides the load-carrying capacity to the connection and the bond failure of adhesive defines the end of the first stage; in the second stage, adhesive is lost and the bolts start to carry the load; and in the third stage, the cracks keep propagating and the displacement of connection increases rapidly, resulting in the ultimate failure of the connection. Hai studied the tensile behavior of double-lap hybrid connections to pultruded hybrid CFRP/GFRP laminates [25]. A quasi-plastic behavior of the connection was seen, while in this test, the behavior of the connection was divided into four stages.

In addition, the structural performance of the bolted connections in GFRP structures is found to be affected by the fiber direction, stacking sequence, dimensions and clamping pressure [26], while the behavior of adhesive bonded connections are influenced by the surface roughness, bonding thickness, fillets, environmental conditions and connection dimensions [27,28]. These parameters, together, have an impact on the strength and stiffness of hybrid connections. Hai studied the influence of connection dimensions on the strength and failure modes of hybrid connections [25]. It was found that when the edge distance—distance between the center of bolt hole and the edge of connecting plate—was small, the shear failure of the plate could lead to the ultimate failure of connection; when the edge distance was increased, the pin-bearing strength of bolt hole would control the ultimate failure mode.

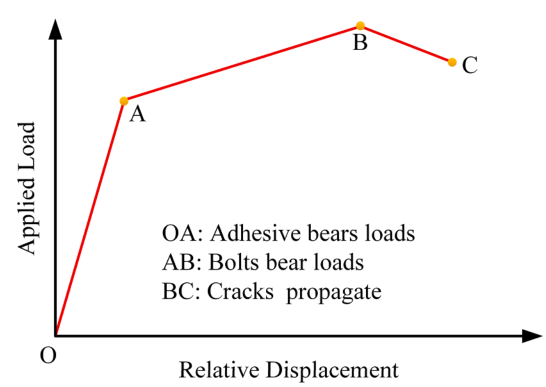

Fig. 1. Multi-stage behavior of hybrid connection [21].

In addition, Kelly addressed the influence of four parameters on the behavior of connection, including the adhesive thickness, overlap length, pitch distance and adhesive modulus [21]. It was found that the relative stiffness of the bolt and adhesive bonding determined the load redistribution. Furthermore, Kelly also investigated the performance of hybrid composite single-lap connections with different adhesives [29]. It was shown that a stiff epoxy adhesive offered a limited improvement, and the fatigue life of connection was mainly determined by the bolt.

Many analytical studies have also been conducted so as to address the structural behavior and develop the design methods for the hybrid connections in GFRP structures. Barut et al. developed a semi-analytical method for the coupled in-plane and bending analysis of composite bonded-bolted single-lap hybrid connections [30]. With this method, it is assumed that the load is initially transferred through the adhesive, and the bolts do not carry the load until the adhesive layer is deboned. In addition, Bios et al. developed a semi-analytical 1-D model for the double-lap hybrid connection [31]. This model considered the nonlinear behavior of epoxy resin and multiple failure criteria, and thus, is able to predict the strength and stiffness of the hybrid connections with single bolt under tensile load. Recently, Paroissien et al. proposed a simplified method to analyze the load transfer in single-lap hybrid connections [32]. The bilinear damaging evolution was considered for adhesive, and the multi-modes critical energy release rates were used to predict the damage of composites. From previous studies, it can be concluded that hybrid connections have a good mechanical performance for pultruded GFRP beams and columns. In order to further expand the scope of FRP structures, this work is conducted on a full-scale hybrid connection that is capable of providing moment resistance for large-scale GFRP structures such as bridges and frame structures.

In this work, an adhesive-bolt hybrid connection was studied. Connection configuration simulated a typical beam-column connection at a corner column in a pultruded GFRP frame structure (see Fig. 2). This type of connection is able to carry moment and shear force, and cyclic load in earthquake. Experimental tests were conducted to study the flexural and shear behaviors of connection under various load conditions, including monotonic and cyclic loadings. In addition, three shear-span ratios were used in the tests to study the influence of shear force, since shear failure is commonly known as a weakness of GFRP materials. In the end, analytical model was carried out to predict the flexural performance of hybrid connection.

2. Experimental study

2.1. Specimen

In this work, a series of experimental program was conducted to investigate the flexural and shear behaviors of the adhesive-bolt hybrid connection under monotonic and cyclic loading. As shown in Fig. 2, two GFRP channel-sections (C-sections), having geometries of 300 × 80 × 18 mm ($h \times b \times t$), simulated the beam of a frame structure. Two rectangular box-sections, having geometries of 230 × 153 × 8 mm ($h \times b \times t$), simulated the corner column of a large-scale frame. Two box-sections were directly attached to each other using epoxy resin. In addition, two C-sections were attached to box-sections through steel bolts and epoxy resin adhesive. Surface treatment was conducted using a sanding machine at the webs of the GFRP C- and box-sections being connected before applying adhesive. Totally, 12 standard size M14 Grade A2-70 stainless steel bolts having diameter of 14 mm, tensile strength of 552 MPa and yield strength of 442 MPa were used, 6 for each box-section. The diameter of bolt holes was 16 mm, with the clearance of 2 mm. In order to fasten the bolts and eliminate the possible stress concentration at the webs of GFRP C- and box-sections being connected, 12 GFRP tubular sleeves, one for each bolt, were used inside of the box-sections as web stiffeners, providing an extra support to the webs as well as ensuring no local damage occurs when fastening bolts to desired strength. Again, epoxy resin was used to fill the gap between steel bolt and GFRP sleeve. Steel bolts were tightly fastened by a torque of 50 Nm.

At the interface of webs of C- and box-sections, epoxy resin adhesive was applied and cured for 2 h. Material characterization tests were conducted to evaluate the mechanical properties of the GFRP and epoxy resin adhesive. The results are summarized in Table 1.

2.2. Experimental setup

Test set-up was designed to model a typical exterior/side connection in a frame structure (see Fig. 3). Horizontal rectangular box-sections were fixed at left end through steel sleeve and bolts, and horizontally loaded at the right end using a hydraulic jack, providing a constant axial compression load, 35 kN, to simulate the load at a column. Lower ends of the two C-sections were connected to box-sections by bolts and adhesive, while their upper ends were connected to a horizontal MTS

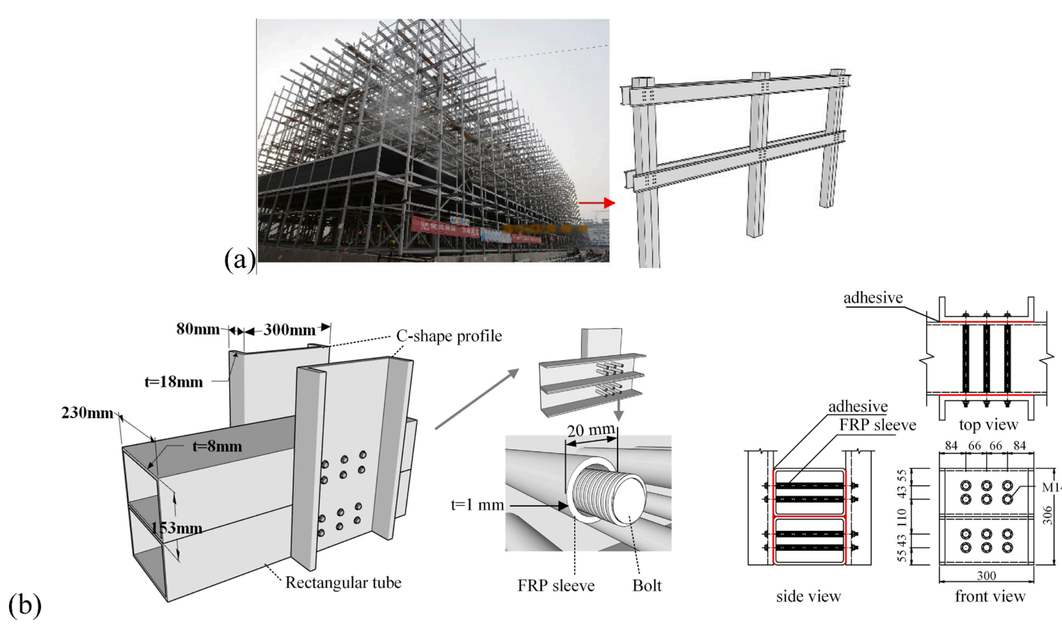

Fig. 2. Adhesive-bolt hybrid connection (mm): (a) Typical beam-column connections in a FRP frame structure and (b) Schematic configuration of adhesive-bolt hybrid connection.

Table 1
Mechanical properties of pultruded GFRP and epoxy resin.

Material	Property	Value	COV	Test method
GFRP	Longitudinal tensile modulus E_L^t (MPa)	41,210	0.01	ASTM D3039
	Longitudinal tensile strength f_L^t (MPa)	650	0.01	
	Transverse tensile modulus E_T^t (MPa)	9140*	–	
	Transverse tensile strength f_T^t (MPa)	32	0.09	
	Longitudinal compressive modulus E_L^c (MPa)	33,918	0.08	ASTM D695
	Longitudinal compressive strength f_L^c (MPa)	457	0.07	
	Transverse compressive modulus E_T^c (MPa)	8709	0.06	
	Transverse compressive strength f_T^c (MPa)	126	0.01	
	Longitudinal bolt hole bearing strength $f_{c,L}$(MPa)	272	0.03	ASTM D953
	Transverse bolt hole bearing strength $f_{c,T}$ (MPa)	231	0.07	
	Major Poisson's ratio ν	0.30	0.18	ASTM D3039
epoxy resin	shear strength τ_m (MPa)	3.5	0.05	ASTM D5868
	shear modulus G_m (MPa)	380	0.07	

* Two effective test results were obtained and used in the calculation of mean value.

electrohydraulic servo tester, through which monotonic and cyclic loads can be generated at the connection. Servo tester had a maximum compression capacity of 1460 kN, a maximum tension capacity of 960 kN, and a maximum stroke of 500 mm (i.e., 250 mm in '+' and '–' directions). Both monotonic and cyclic loadings were controlled at a rate to ensure the static behavior of connection. A sliding hinge restraint was set 1.3 m away from the rotational center of the connection to further eliminate the possible vertical displacement of the box-sections. The other fixed end was set 0.5 m away from rotation center. This boundary set-up is to simulate a typical exterior/side beam-column connection in a GFRP frame structure.

In order to study the influence of shear load, six specimens, divided into three groups based on different shear-span ratios (two specimens in each group), were tested. Shear-span ratio (λ) was calculated as $\lambda = a/h$, where a was the length of the lever arm, and h was the section height of the GFRP C-sections. In each group, one specimen was tested under a monotonic load and the other was tested under a cyclic load. Specimen configuration is presented in Table 2.

Monotonic loading was conducted by displacement-control; that is, load was applied to the specimen at a constant displacement rate of 2 mm/min until failure occurred. In monotonic loading tests, quasi-yield load (P_y) was obtained from moment-rotation curve and the elastic range of the specimens can be identified. In addition, farthest point method was used to determine the quasi-yield load when it cannot be observed from moment-rotation curve (see Fig. 4) [33]. In cyclic loading tests, specimens were loaded in displacement-control until failure. The cyclic loading scheme was determined in accordance with Chinese standard JGJ 101 [34]. The level of load started from θ_y, which is the quasi-yield rotation measured from the monotonic test and incremented at a step size of θ_y. Each load was repeated twice. That is, the loading cycles started from θ_y, and then went to $2\theta_y$, $3\theta_y$, $4\theta_y$, $5\theta_y$, until failure of the connection. Despite of the difference between Chinese standard JGJ 101 and ATC-24 [35], following JGJ 101 the cyclic response of the connection can be satisfactorily assessed.

2.3. Instrumentation

The instrumentation to measure the displacement and strain of the specimen is shown in Fig. 3b and 3c. Four LVDTs, H1, H2, H3 and H4, with a stroke of 500 mm, were evenly placed at one side of the C-sections so as to measure their horizontal displacements (see Fig. 3b). In particular, H1 was placed at the center of connection to measure the displacement of the connection. In addition, two LVDTs, V1 and V2, with a stroke of 50 mm, were placed at the center of the connection and at 0.5 m away from the edge of the rectangular box-sections (see Fig. 3b), measuring the possible vertical displacements of the box-sections. Moreover, three LVDTs, D1, D2 and D3, with a stroke of 50 mm, were placed near steel sleeve to measure the possible deformations of the steel sleeve (see Fig. 3c). Six 120 ohm strain gauges (S1-S6) with a gage area of 10.0 × 2.0 mm (length × width) were installed at the webs of box-sections, and seven 120 ohm strain rosettes (S7-S13) with a gage area of 3.0 × 2.0 mm (length × width) were installed near the bolts (see Fig. 3d).

3. Experimental results

3.1. Monotonic loading test

Monotonic loading tests were conducted on specimens, FS-1, FS-2 and FS-3. A typical failure mode (FS-2) is shown in Fig. 5. It can be seen that the webs of the C- and box-sections were cracked in their longitudinal directions, along with the bolt lines (see Fig. 5a). Such cracks initiated at bolt holes; that is, bolt hole bearing failure occurred first (see Fig. 5b). It is noted that before the crack initiated in webs, the adhesive layers between webs of C- and box-sections were fractured completely. Findings observed in each test are presented in following sections.

In the test on FS-1, the first micro-cracking was heard at a load of 16 kN and no noticeable crack was found on specimen, and the hybrid connection continued to deform in a linear manner. Then, adhesive layer started to crack at a load of 118 kN and a relative rotation between the C- and box-sections was observed. With the adhesive layer completely failed, a crack was found at the web of the lower box-section—at the bottom left corner of the connection region—at a load of 140 kN. Then, more cracks showed up and propagated rapidly, leading to failure of the entire connection, which was similar to the experimental observations reported by Feroldi et al. [36]. Specimen was found to reach its peak load at 144 kN. When the first crack occurred at the web of a box-section, horizontal displacement (H4) was 32 mm (0.064 rad). Test stopped at a displacement (H4) of 72 mm (0.144 rad). After unloading, the residual rotation was 0.064 rad.

For FS-2, the first micro-cracking was heard at a load of 22 kN, and similarly to FS-1, no crack can be seen on the specimen and the connection continued to deform linearly. The adhesive layer completely failed at the load of 64 kN, and then, vertical C-sections started to crack at a displacement (H4) of 43 mm (0.043 rad). Load was found to drop from 72 kN to 47 kN. Nonetheless, cracks stopped propagating at 47 kN and the load continued to increase to 71 kN. Horizontal box-sections were found to crack at a displacement (H4) of 113 mm (0.113 rad). Test stopped at a displacement (H4) of 170 mm (0.170 rad), and the C-sections reached a rotation of 0.036 rad. Horizontal cracks on box-sections had a maximum width of 15 mm and a maximum length of 510 mm. The vertical cracks on C-sections extended throughout their length.

In the test on FS-3, noticeable cracking was heard twice: at displacements (H4) of 26 mm and 32 mm (rotations of 0.017 rad and 0.021 rad). Nonetheless, the connection was still able to carry more load. The stiffness, however, slightly reduced after the observed cracking. This was due to the damage of adhesive layer. Then, steel bolts took over the load. The box-sections finally cracked at a displacement (H4) of 86 mm (0.057 rad).

For the three specimens with different shear-span ratios, the failure modes were found to be similar, which can be characterized using a multistage damage mode similar to that proposed by Kelly [21], as shown in Fig. 6. Based on the box-section strains measured from gauges S1-S6 (see Fig. 7), a linear strain distribution was found before the

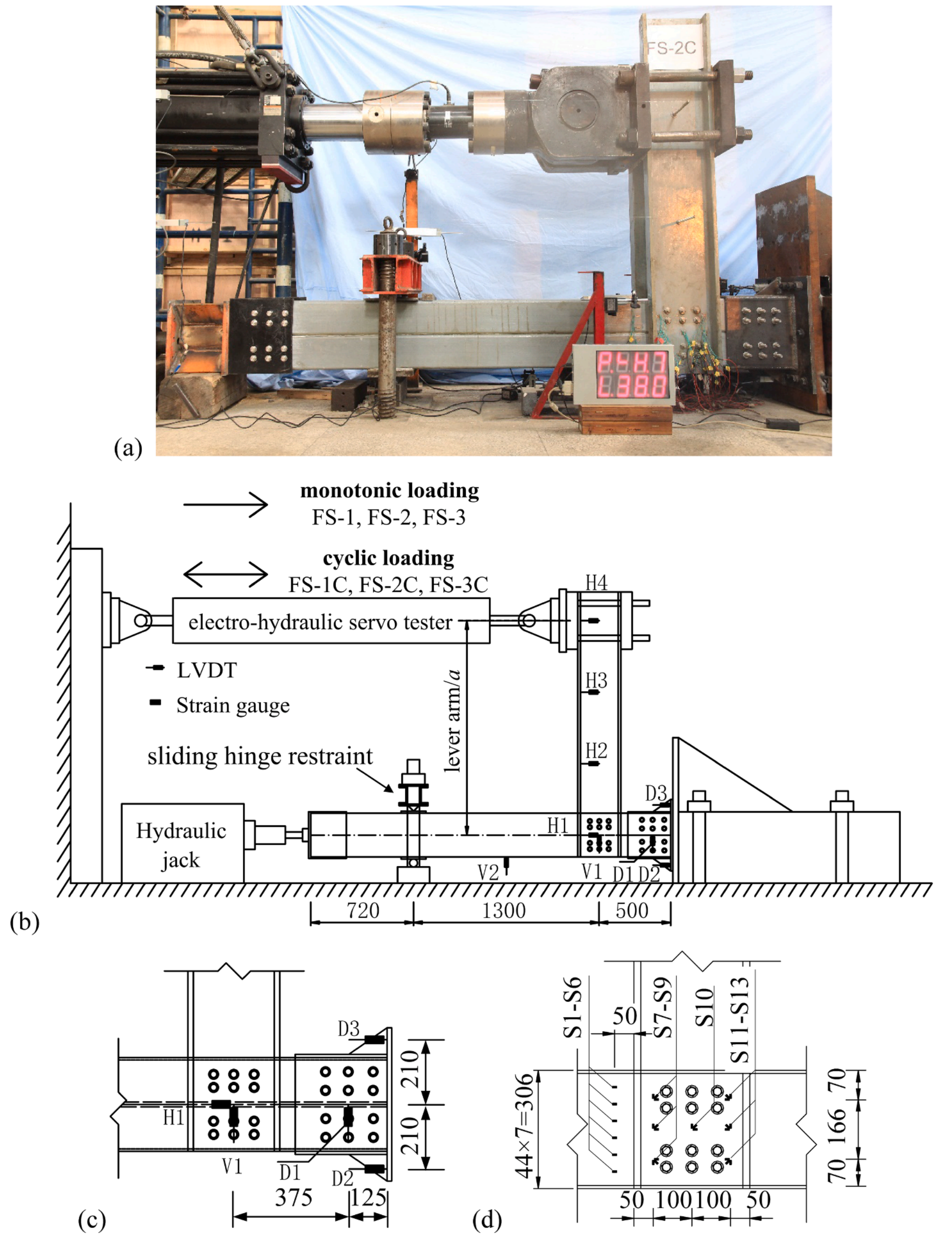

Fig. 3. Test configuration: (a) Test set up; (b) Schematic of test set-up; (c) LVDTs at steel cuff (D1-D3) and center of C-section (H1 and V1); (d) Strain gauges at webs of box-sections (S1-S6) and around bolt holes at connection zone (S7-S13) (mm).

Table 2
Specimen configuration.

Label (1)	Lever arm in m (2)	Section height *h* in mm (3)	Shear-span ratio (4)	Loading pattern (5)
FS-1	0.5	300	1.7	Monotonic loading
FS-1C	0.5	300	1.7	Cyclic loading
FS-2	1.0	300	3.3	Monotonic loading
FS-2C	1.0	300	3.3	Cyclic loading
FS-3	1.5	300	5.0	Monotonic loading
FS-3C	1.5	300	5.0	Cyclic loading

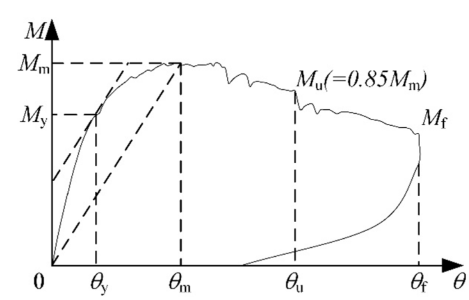

Fig. 4. Yield point defined by the Farthest Point Method [33].

adhesive layer was completely failed, and thus, the plane-section assumption near the connection region was validated. However, plane-section assumption did not hold when adhesive layer was damaged and stress concentration occurred. With cracks occurred and propagated, a quasi-plastic behavior of the connection was observed.

Moment-rotation curves of the three specimens under monotonic loads are shown in Fig. 8. The horizontal displacements at the different heights, measured by LVDTs H2, H3 and H4, were used to calculate the

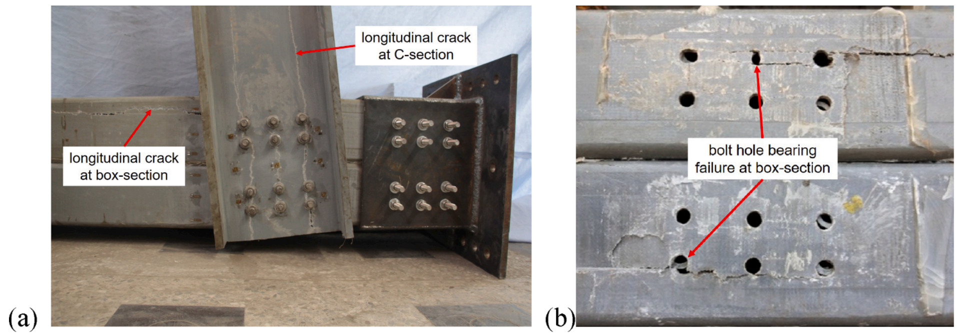

Fig. 5. Typical failure mode (FS-2 shown as an example): (a) Longitudinal cracks along bolt lines; (b) Bolt hole bearing failure of box-sections after adhesive layer failed.

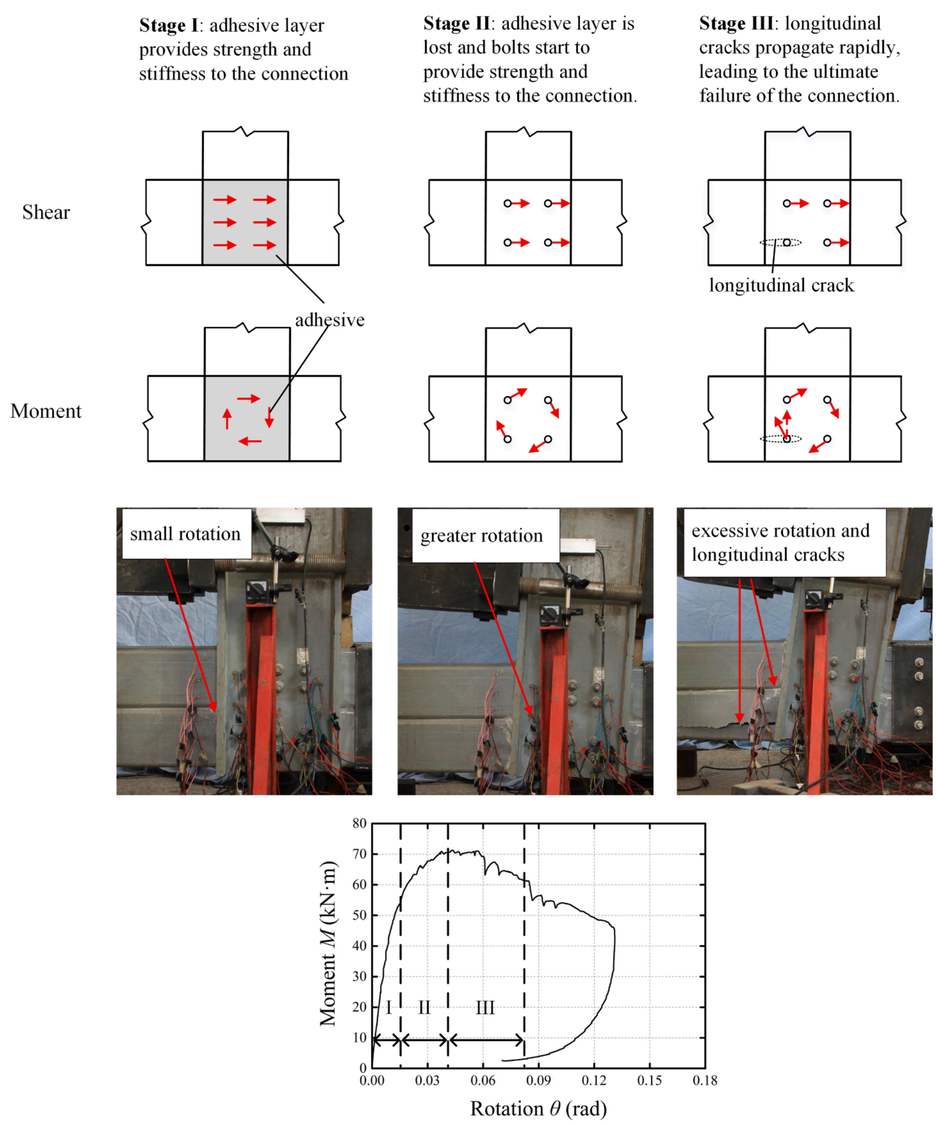

Fig. 6. Observed multistage damage of the hybrid connection (FS-1 shown as an example).

rotations of the connection. Calculated rotations were found to be close to each other; that is, the "sufficient stiffness" of the C-section is validated. In addition, Connection rotations calculated using readings of LVDTs at different heights were found to be close to each other.

As shown in Fig. 8, each specimen exhibited a relatively large deformation before completely failed. Although GFRP composites are typically deemed as an elastic material, this hybrid connection, as a structural component, clearly showed quasi-plastic deformation. The bearing failure at bolt holes as well as the longitudinal cracks at webs of the C- and box-sections led to a large rotational deformation. Adhesive layer is found to be able to provide a high stiffness to the connection, and the steel bolts can continue to carry the load after the adhesive layer was lost.

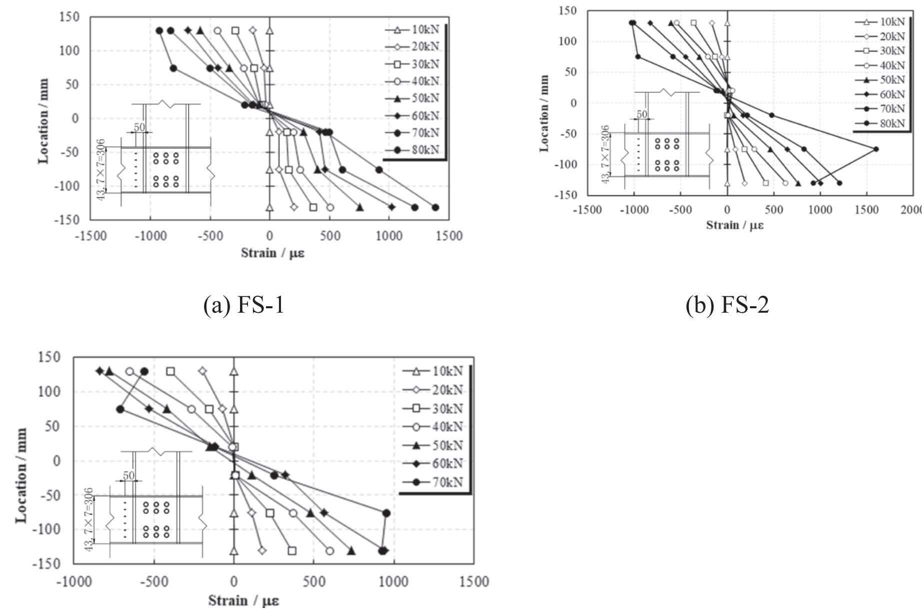

Fig. 7. Strain distribution of box sections: (a) FS-1; (b) FS-2; (c) FS-3.

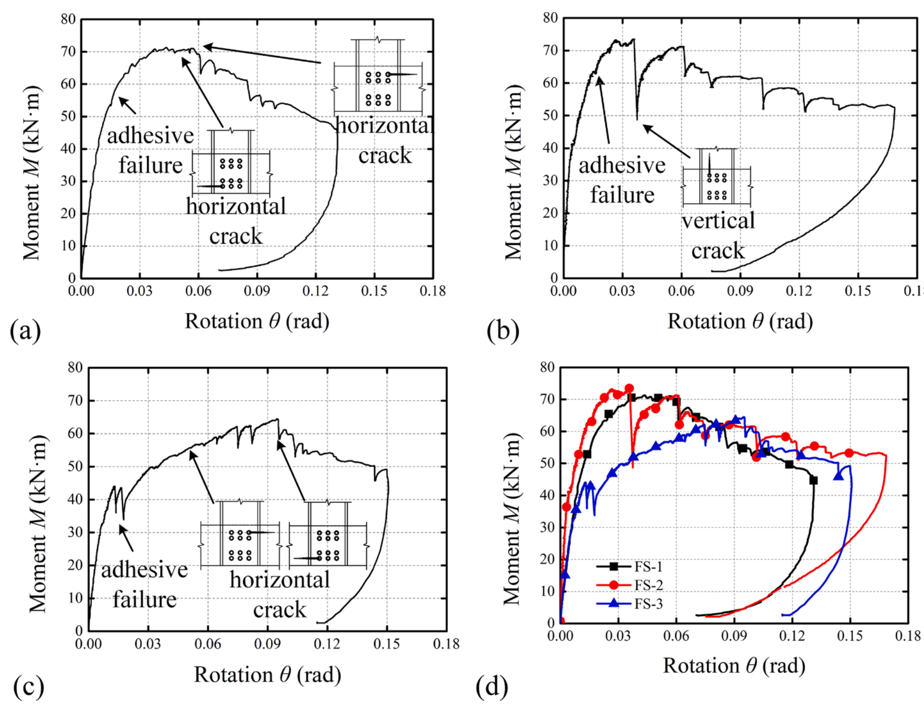

Fig. 8. Moment-rotation curves of monotonic loading tests: (a) FS-1; (b) FS-2; (c) FS-3; (d) Comparisons.

3.2. Cyclic loading test

Three specimens, FS-1C, FS-2C and FS-3C, were tested in cyclic loading. Similarly to specimens in monotonic loading tests, FS-1C, FS-2C and FS-3C showed a linear relationship between moment and rotation until adhesive layers failed at 43 kNm, 53 kNm, 42 kNm in pushing direction (noted as + direction) and 40 kNm, 50 kNm, 44 kNm in pulling direction (noted as - direction), respectively.

After adhesive layer failed, the stiffness of connection decreased, and the rotation increased rapidly. GFRP C- and box-sections began to crack as displacement increased. FS-1C, FS-2C, and FS-3C were found to have their first cracks at loads of +60 kNm, +65 kNm, and −64 kNm, respectively. With the cracks propagated, the load decreased. Peak loads of FS-1C, FS-2C, and FS-3C were −77 kNm, +68 kNm, and −62 kNm, respectively. In particular, FS-3C had smallest peak load due to the premature crack of adhesive layer. At the beginning of unloading process, the unloading stiffness, obtained from moment and rotation curves, was close to loading stiffness. As unloading process continued, unloading stiffness gradually decreased and a residual deformation was observed.

Fig. 9 shows the moment-rotation curves measured by different LVDTs of monotonic loading tests. The curves reflect the influence of member flexural deformation. The figure shows that three curves are close, so the member flexural deformation is little and can be ignored.

Moment-rotation curves for the three specimens under cyclic loading are shown in Fig. 10. Compared to the monotonic load tests, the cyclic loading led to more cracks and greater deformations. In addition, asymmetric crack pattern in specimens in cyclic loading tests may lead to a slight difference between rotation in + and − directions. This phenomenon is more prominent in FS-2C.

Skeleton moment-rotation curves of the cyclically loaded specimens were also obtained, as shown in Fig. 11a. In addition, these skeleton curves were compared with the moment-rotation curves of the three monotonically loaded specimens (see Fig. 11b, c and d). It can be seen that the skeleton curves from cyclic loading tests have a similar trend with the moment and rotation curves from monotonic loading tests, indicating that loading scheme has little impact on the flexural behavior of hybrid connection.

3.3. Summary of results

From the experimental results, it is seen that the measured vertical displacements at V1 and V2 were less than 1 mm in all tests, indicating the flexure of box-sections can be neglected. Thus, the specimens tested in monotonic loading (FS-1, FS-2 and FS-3) can be considered as the same three specimens repeatedly tested three times; and the same conclusion also holds for the cyclic test. The measured loads and rotations of both monotonically loaded specimens and cyclically loaded specimens are presented in Table 3. In order to compare this result with other kinds of connections, a dimensionless parameter η related with connection effectiveness is calculated and listed in Table 3. This parameter is obtained by dividing the maximum experimental moment M_m and the theoretical bending capacity of the beam profile M_b. The M_b of C-shape profile is calculated by ASCE standard, as shown in Eq. (1). Resistance factor or time effect factor is not considered.

$$M_b = \frac{F_L I}{y}, \tag{1}$$

where F_L is the characteristic longitudinal strength; I is moment of inertia of the member about the axis of bending; y is distance from the neutral axis to the extreme fiber of the member. According to Eq. (1), the theoretical bending capacity of C-shape beam is 259 kNm. Then the connection effectiveness η can be calculated.

It can be seen that the quasi-yield moments of FS-1, FS-2 and FS-3 are similar: average quasi-yield moment is 43 kNm with COV of 0.01. On the other hand, FS-1C, FS-2C and FS-3C in pushing (+) and pulling (−) processes were also close: the average quasi-yield moment is 45 kNm with COV of 0.01.

In addition, when comparing all six specimens, it is found that the average quasi-yield moment is 45 kNm with COV of 0.09, further demonstrating that the loading scheme, monotonic or cyclic loading, also has little influence on the flexural behavior.

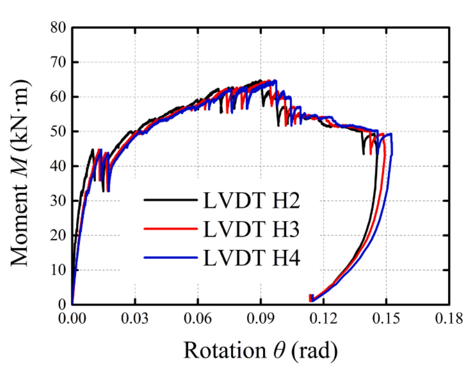

Fig. 9. Moment-rotation curves measured by different LVDTs of monotonic loading tests (FS-3 shown as example).

Calculating the average maximum load of all six specimens yields a flexural strength of 67 kNm and a COV value of 0.09. All specimens reached the ultimate moment with an ultimate rotation greater than 0.083 rad. That is, the hybrid connection is capable of retaining most of the moment resistance at a relatively large rotational deformation. All six connections are found to be able to behave in a quasi-plastic manner and had a factor of rotational ductility larger than 4.8.

4. Analytical study

4.1. Multistage behavior

From the experimental results obtained in this work, the moment and rotation relationship of the adhesive-bolt hybrid connection can be divided into three stages: (1) elastic stage, (2) quasi-plastic stage, and (3) softening stage. In elastic stage, connection rotation has a linear relationship with the applied moment. In this stage, no damage occurs to adhesive or GFRP profiles. In addition, adhesive layer has a high stiffness, and steel bolts are not in full contact with GFRP profiles when adhesive layer is intact. Adhesive layer, therefore, is to carry the entire load in elastic stage. In quasi-plastic stage, the adhesive layer starts to crack and the stiffness of the connection decreases. In addition, the bolts start to carry the load and bearing failure at bolt holes may occur. In softening stage, the moment resistance of the connection starts to decrease, while the rotation of the connection increases rapidly. The connection finally fails due to the excessive cracks in GFRP profiles and the sudden drop of load-carrying capacity of the connection. It is noted that in some cases the local instabilities of GFRP profiles might also lead to the failure of the connection. Nonetheless, such type of failure mode was not observed in this work. The studies by other researchers [37–42] are recommended as a reference to local instability-related failure modes. In this work, experimental observations are respected and accordingly, design equations were derived with regard to the material strength limit states of GFRP profiles and adhesive layers so as to predict the quasi-yield and the maximum moment capacities of the proposed connection.

4.2. Quasi-yield moment

In stage I, the adhesive layer is to carry the load. Therefore, the quasi-yield moment of the hybrid connection can be calculated only considering the adhesive. In formulation for quasi-yield moment, three assumptions are made. (1) Adhesive layer provides the moment resistance to the connection through shear stress before connection yields, while the strength and stiffness of the bolts are neglected. (2) Shear stress is distributed across the entire connection region and proportionally increased from zero at the rotational center to the highest at the corner of the connection region; that is, a linear elastic behavior of adhesive layer. Although such assumption may differ from some of the reported results, such as that by Bios et al. [31], a finite element analysis was conducted (presented in the following section) and it is found that a small deflection would occur when quasi-yield moment of the connection is reached and thus, the nonlinear stress distribution has little effect on the structural performance of the connection. Additionally, using this assumption is demonstrated to be able to yield a conservative prediction of quasi-yield moment capacity. (3) Connection is considered as yielded when the maximum shear stress in the adhesive layers reaches the shear strength of the adhesive. In this case, the maximum shear stress is located at the corner of joint region. So the quasi-yield moment is according to the status that the shear stress of adhesive at corner point reaches shear strength. The quasi-yield moment of the connection is calculated as:

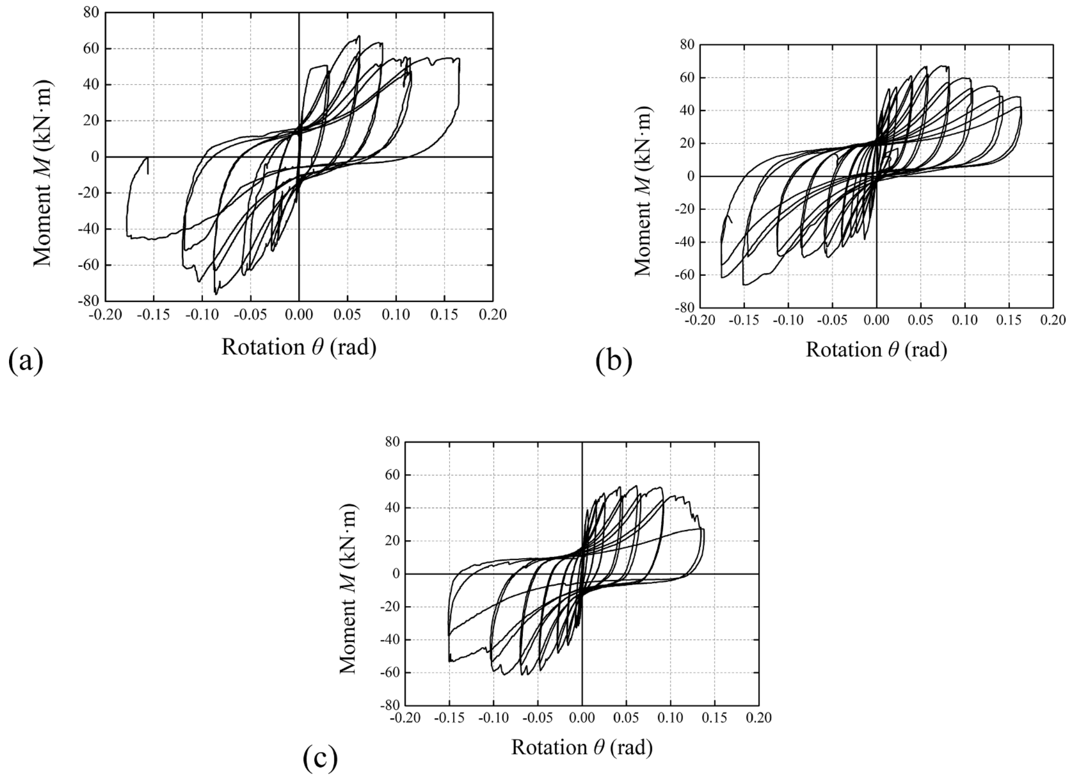

Fig. 10. Moment-rotation curves of cyclic loading tests: (a) FS-1C; (b) FS-2C; (c) FS-3C.

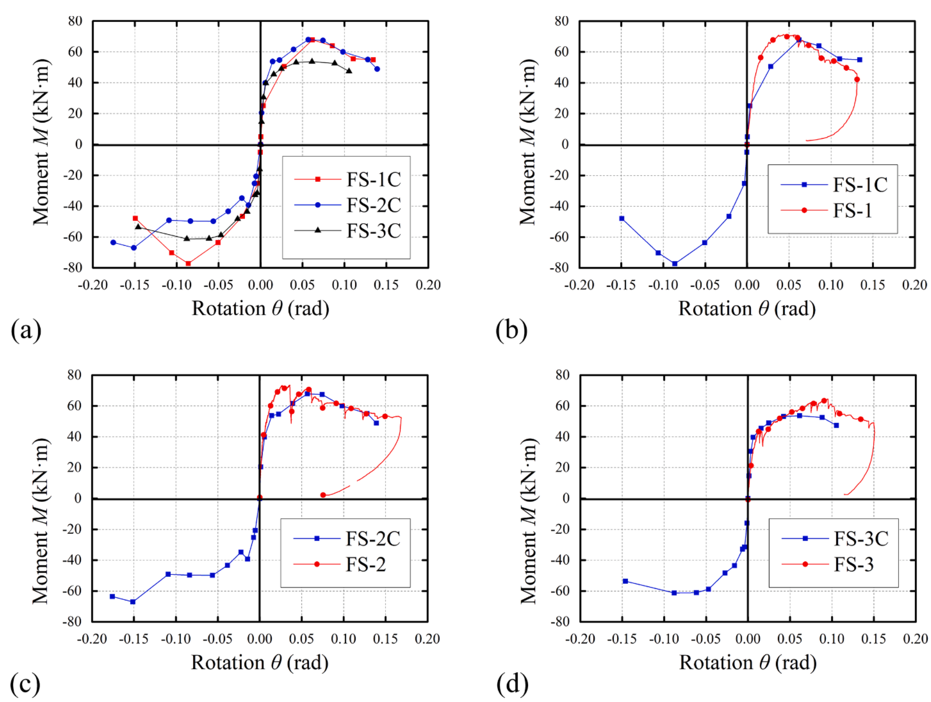

Fig. 11. Skeleton moment-rotation curves of cyclic loading tests and comparisons with monotonic loading tests: (a) Skeleton curves of FS-1C, FS-2C, FS-3C; (b) FS-1C and FS-1; (c) FS-2C and FS-2; (d) FS-3C and FS-3.

$$M_y = \frac{\tau_m}{6r}\left(bh^3 + hb^3\right), \tag{2}$$

where τ_m is the shear strength of the adhesive; r is the distance between the corner of the adhesive zone and the rotational center; and b and h are the width and depth of the adhesive zone, respectively.

4.3. Maximum moment

When the applied moment exceeds the quasi-yield moment, the adhesive layer is deemed as completely lost, and the connection stiffness starts to decrease. In this stage, connection exhibits quasi-plastic deformation. In addition, three assumptions are made. (1) Shear

Table 3
Experimentally determined quasi-yield and maximum moment capacities and ductility factors.

Specimen	M_y (kNm)	θ_y (rad)	$K_{\theta,e}$ (kNm)	M_m (kNm)	θ_m (rad)	θ_u (rad)	M_f (kNm)	θ_f (rad)	μ_θ*	η
FS-1	43	1/112	4704	71	1/23	1/12	44	1/8	9.5	0.27
FS-2	43	1/217	9348	74	1/28	1/10	53	1/6	21.7	0.29
FS-3	44	1/79	3463	65	1/12	1/11	43	1/8	7.7	0.25
FS-1C	+43	1/56	2391	+68	1/16	1/12	+55	1/6	4.8	0.26
	−40	1/71	2856	−77	1/12	1/10	−45	1/6	7.1	0.30
FS-2C	+53	1/67	3535	+68	1/18	1/9	+42	1/6	7.1	0.26
	−50	1/58	2880	−67	1/7	1/6	−63	1/5	10.1	0.26
FS-3C	+42	1/59	2470	+54	1/16	1/9	+23	1/7	6.7	0.21
	−44	1/53	2314	−62	1/15	1/7	−53	1/7	7.9	0.24

* Ductility factor μ_θ is equal to the ratio of ultimate rotation θ_μ (corresponding to 0.85 M_m) to yield rotation θ_y.

resistance of bolts provides the resistance of connection and adhesive layer is neglected. (2) Shear stress at the bolt is in direct proportion to the distance between bolt and rotational center. (3) Bolt is deemed as failed when either pin-bearing stress at bolt hole reaches pin-bearing strength of the GFRP sections or shear stress reaches shear strength of bolts. In addition, the longitudinal bolt hole bearing strength of the GFRP sections is used when angle between shear resultant and longitudinal direction of GFRP section is less than 5 degrees; otherwise, transverse bolt hole bearing strength is used in the calculation, which is determined in accordance with the pin-bearing strength prescribed by ASCE pre-standard [11].

According to above three assumptions, the maximum moment resistance M_m is the summation of moment capacity contributed by every bolt, which can be calculated as:

$$M_m = \sum_{i=1}^{n} V_{u,i} r_i \tag{3}$$

In which, r_i is the distance between rotational center and bolt; $V_{u,i}$ is defined as the minimum value of the bolt hole bearing strength and the shear strength of the ith bolt, as:

$$V_{u,i} = min\{V_{br,i}, V_{bt,i}\} \tag{4}$$

$$V_{br,i} = \begin{cases} f_{c,T} t d_i sec(\alpha) \alpha \geq 5^\circ \\ f_{c,L} t d_i csc(\alpha) \alpha < 5^\circ \end{cases}, \tag{5}$$

$$V_{bt,i} = n_v f_v^b \left(\pi d_i^2/4\right), \tag{6}$$

where $V_{br,i}$ is the bolt hole bearing strength of the ith bolt; $V_{bt,i}$ is the shear strength of the ith bolt; t is the thickness of the GFRP sections being connected; α is the angle between stress at ith bolt and pultrusion direction, as shown in Fig. 12; d_i is the diameter of the bolt; $f_{c,T}$ is the transverse bolt hole bearing strength of the GFRP sections; $f_{c,L}$ is the longitudinal bolt hole bearing strength of the GFRP sections [11]; n_v is

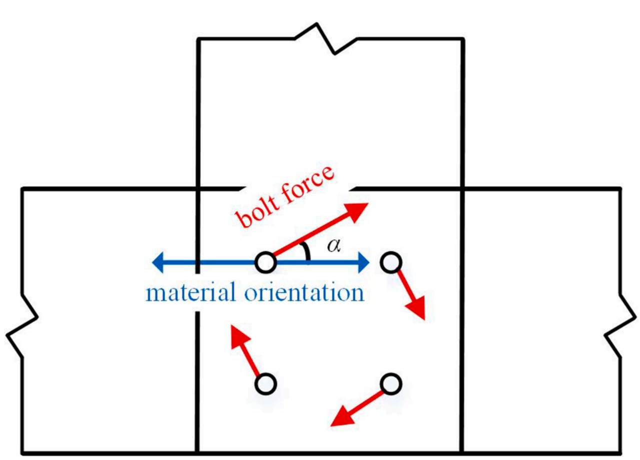

Fig. 12. Definition of alpha α.

the number of shear interface in bolts; and f_v^b is shear strength of bolts; sec function is the reciprocal of cosine; csc function is the reciprocal of sine.

4.4. Validation

Table 4 shows the predicted quasi-yield and maximum moment capacities of all specimens. The predicted moments were compared with the experimental results obtained in this work. It can be seen that the proposed equation (Eq. (2)) could provide generally conservative quasi-yield moment capacity for the hybrid connection addressed in this work. On the other hand, for the maximum moment capacities, except for specimen FS-3C that shows a premature failure, a good agreement is found between experimental results and predictions, having the greatest difference less than 11%. Thus, it can be concluded that using proposed equation, the quasi-yield and maximum moment capacities can be obtained.

4.5. Equivalent viscous damping ratio

In order to evaluate the seismic performance of the hybrid connection, the equivalent viscous damping ratio, ζ, was calculated using the method proposed by Rodrigues [43].

$$\zeta = \frac{1}{4\pi}\frac{E_D}{E_{SO}}, \tag{7}$$

where E_D is the dissipated energy by damping of connection; and E_{SO} is the dissipated energy by nonlinear behavior of connection. In hysteretic curves, E_D is the area of one hysteretic cycle, as shown in the shaded area in Fig. 13, and E_{SO} is the area of the triangle under maximum load point.

This damping ratio is calculated as the ratio between the dissipated energy by damping and the energy dissipated by nonlinear behavior in every load cycle. In addition, damping ratio is in proportion to the secant stiffness of connection in elastic phase [44]. The damping ratio typically describes the post yielding characteristics of the structure, and in this work, it reflects the performance of connection when adhesive was lost and quasi-yield moment was achieved.

The calculated equivalent viscous damping ratios of the cyclically loaded specimens, FS-1C, FS-2C and FS-3C, are presented in Fig. 14. Despite of the variances among cycles and specimens, it is seen that the tendencies of three specimens are similar. Indeed, all three specimens are found to have similar equivalent viscous damping ratios of 0.20. When compared to the conventional structures, such as the reinforced concrete column having a similar ductility factor and a damping ratio of 0.25 [43], the hybrid connection showed a good energy dissipation capacity.

5. Finite element modeling

A finite element model (FEM) was built via ABAQUS to simulate half of the structure [45], as shown in Fig. 15. In this model, shell elements (S4) were used in C- and box-section GFRP profiles. Hashin damage

Table 4
Analytically and numerically determined quasi-yield and maximum moment capacities.

Specimen	Quasi-yield moment capacities					Maximum moment capacities				
	M_{exp} (kNm)	M_{FEM} (kNm)	*FEM*/exp	M_{pred} (Eq. (2)) (kNm)	*pred*/exp	M_{exp} (kNm)	M_{FEM} (kNm)	*FEM*/exp	M_{pred} (Eq. (3)) (kNm)	*pred*/exp
FS-1	43	46	1.07	41	0.97	71	69	0.97	73	1.03
FS-2	43	44	1.02	41	0.95	74	67	0.91	73	0.98
FS-3	44	43	0.98	41	0.94	65	63	0.97	73	1.11
FS-1C	+43	–	–	41	0.96	+68	–	–	73	1.07
	−40	–	–	41	1.03	−77	–	–	73	0.94
FS-2C	+53	–	–	41	0.78	+68	–	–	73	1.07
	−50	–	–	41	0.82	−67	–	–	73	1.08
FS-3C	+42	–	–	41	0.98	+54	–	–	73	1.34
	−44	–	–	41	0.93	−62	–	–	73	1.17

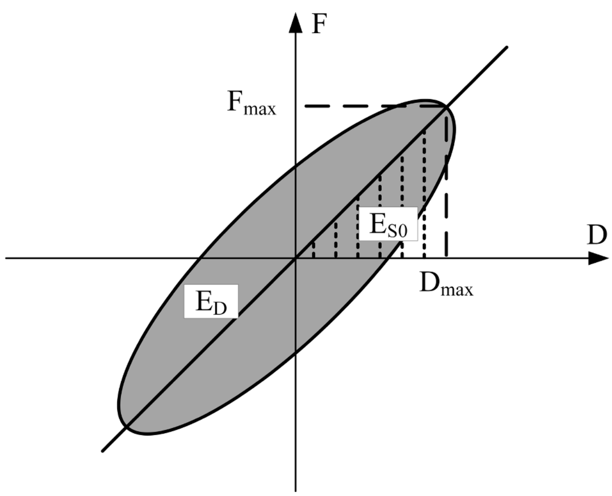

Fig. 13. Energy dissipated in a one hysteresis loop.

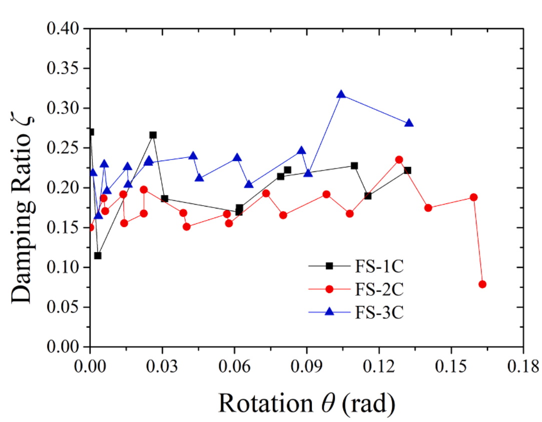

Fig. 14. Equivalent viscous damping ratio vs. rotation angle of cyclically loaded specimens.

criterion was applied to evaluate the damage of GFRP material. The elastic modulus and strength in Hashin criteria were determined in accordance with those shown in Table 1. Longitudinal tensile and compressive, transverse tensile and compressive fracture energies have values of 3.7, 4.8, 0.4 and 1.7 N/m, respectively. Cohesive elements (COH3D8) were used to simulate the adhesive. The thickness of adhesive was specified as 1 mm. Cohesive elements have initial elastic modulus of 380 MPa and shear strength of 3.5 MPa. Secant modulus was determined in accordance with mechanical test results of the adhesive. Elongation rate of 12% was used in the damage evolution. Solid elements (C3D8), having isotropic elastic modulus of 205 GPa, were assigned to bolts. Clearance of 1 mm was assigned for interaction between bolts and bolt holes. Provided no plastic deformation of bolts was observed in tests, the bolts were modeled with elastic law. In FEM, two loading steps were used. In the first step, axial compression was applied in box-section profiles; and in the second step, horizontal load was applied at the end of C-section profile. Quasi-yield moment and maximum moment capacities of FEM results are listed in Table 4.

Fig. 16 shows the overall deformation and stress distribution at the connection region at two moments, including the quasi-yield moment and the maximum moment. The whole deformation is similar with the test phenomenon. As for the stress distribution, at the quasi-yield moment, the rotational center is approximately located at the center of the connection. It can be seen that the non-linear behavior of adhesive has little influence and the stress is approximately in proportional to the distance from rotation center. At the maximum moment, most of the adhesive was damaged and GFRP is damaged near the bolt holes because of longitudinal compressive and transverse tensile stress.

Fig. 17 shows the comparison between moment-rotation curves of experimental and FEM results. In general, FEM curves of FS-1 and FS-2 have a good agreement with experimental results. For FS-3, quasi-yield moments obtained from experimental test and FEM are close, whereas the rotation stiffness measured in test has abruptly decreased when exceeding the quasi-yield moment. This was due to the fact that FS-3 experienced more damages in the test after quasi-yield moment. In addition, FEM typically has a better performance in loading stage than that in unloading stage. This is mainly attributed to the used element degeneration approach which inevitably has a difference from the actual crack propagation.

6. Discussion and design recommendation

Although a specific test set-up was used in this work, the findings are readily applicable to similar type of the hybrid connections in GFRP structures. Through experimental observations in this work, it is identified that a quasi-plastic behavior of the connection can be achieved by combining adhesively bonded and mechanically bolted connections, though GFRP material is typically a linear elastic material.

In practical constructions, it is recommended to consider only the quasi-yield moment as the design strength of connection in service limit state, thus having the flexural strength of bolted connection as a seismic reserve. When the quasi-yield moment capacity is reached, the connection is still able to carry the load, particularly the cyclic load, further dissipating energy in earthquake and protecting the integrity of the entire GFRP structure.

In addition, in stage I the hybrid connection is recommended to be taken as a rigid connection, as a high stiffness and little rotation were observed in the tests. In stage II the connection exhibited degraded stiffness and greater rotation and thus, a semi-rigid connection is recommended to be considered in designs. Furthermore, in the calculation of maximum moment various failure modes should be considered, such as the bolt hole bearing failure and bolt shear failure addressed in this work as well as those identified in other studies [46,47].

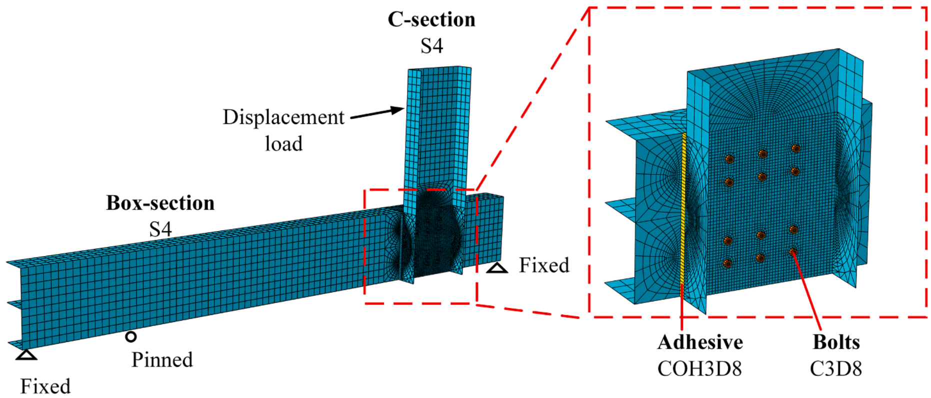

Fig. 15. FEM for the connection.

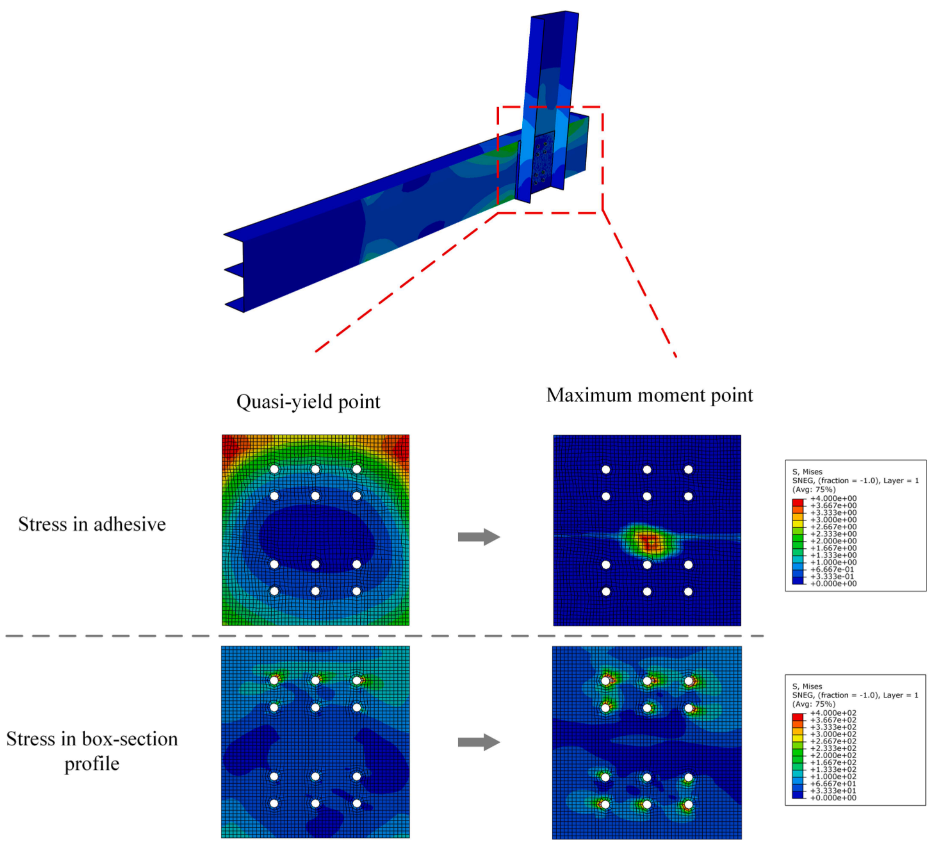

Fig. 16. Deformation and stress distribution at connection region of FEM.

7. Conclusion

In this work, an adhesive-bolt hybrid connection for GFRP structures is addressed. The flexural behavior of the connection is investigated through an experimental program. Design equations are proposed to predict the moment capacities of the connection. A good agreement is found between experimental results and theoretical predictions. Findings and conclusions from this work are summarized in following sections.

(1) Six adhesive-bolt hybrid connections were tested under monotonic and cyclic loading until failure. Specimens showed the same failure mode. That is, crack initiated in adhesive layer, and then, excessive crack occurred at the webs of GFRP sections, leading to the failure of the entire specimen. All cracks at webs are found to form along bolt lines in longitudinal direction of material.

(2) Specimens initially behaved in an elastic manner. After crack occurred in adhesive layers, specimens transitioned into a quasi-plastic behavior. Having quasi-plasticity, the hybrid connection was able to retain the moment resistance, while the rotational stiffness began to decrease. In quasi-plastic stage, complete failure of adhesive layer was first observed. Then, the connection continued to deform with little increase in load, which can be considered as an early warning of approaching the ultimate capacity of the connection.

(3) Specimens showed similar structural behavior under both monotonic and cyclic loading. Skeleton moment and rotation curves for the cyclic loading tests are similar to those from the monotonic loading tests. The average stiffness declined rapidly in

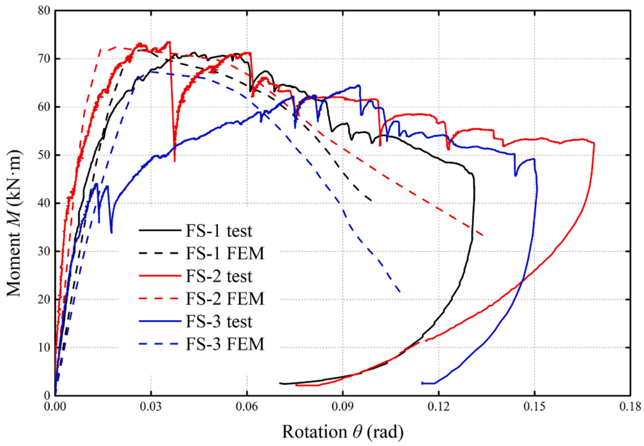

Fig. 17. Moment-rotation curves of experimental and FEM results.

cyclic loading process. Connections showed good performance in terms of the energy dissipation.

(4) Structural behavior of the hybrid connection is divided into three stages: (1) elastic stage, (2) quasi-plastic stage, and (3) softening stage. Design equations are developed to predict the quasi-yield moment and the maximum moment of the hybrid connection in elastic and quasi-plastic stages. A good agreement is found between experimental results and analytical predictions. In addition, the proposed equations were used in design of the connections in a frame.

(5) When yield moment is reached, quasi-plasticity with a reduced stiffness can be considered in design, permitting an improved cost-effectiveness of the project. In addition, quasi-plastic behavior of the hybrid connection could potentially permit the seismic design of GFRP frame structures.

CRediT authorship contribution statement

Peng Feng: Conceptualization, Methodology, Supervision, Project administration, Funding acquisition, Validation, Writing - review & editing. **Yuwei Wu:** Methodology, Investigation, Data curation, Formal analysis, Visualization, Writing - original draft, Writing - review & editing. **Yi Ding:** Methodology, Investigation, Validation, Visualization, Writing - review & editing. **TianQiao Liu:** Data curation, Validation, Writing - review & editing. **Ye Tian:** Investigation, Data curation, Software, Validation.

Declaration of Competing Interest

The authors declare that they have no known competing financial interests or personal relationships that could have appeared to influence the work reported in this paper.

Acknowledgments

This research was supported by the National Key Research and Development Program of China (2017YFC0703000), the National Natural Science Foundation of China (No. 51522807 and No. 51478246), and open fund of National Engineering Research Center on Diagnosis and Rehabilitation of Industrial Building (No. YZA2017Ky01).

References

[1] Keller T. Recent all-composite and hybrid fibre-reinforced polymer bridges and buildings. Prog Struct Eng Mater 2001;3(2):132–40.
[2] Feng P, Wang J, Wang Y, Loughery D, Niu D. Effects of corrosive environments on properties of pultruded GFRP plates. Compos Part B: Eng 2014;67:427–33.
[3] Castellaro S, Russo S. Dynamic characterization of an all-FRP pultruded construction. Compos Struct 2019:1–14. https://doi.org/10.1016/j.compstruct.2019.03.032. ISSN: 0263-8223.
[4] Russo S. Experimental and finite element analysis of a very large pultruded FRP structure subjected to free vibration. Compos Struct 2012;94:1097–105. ISSN: 0623–8223.
[5] Liu W, Feng P, Huang J. Bilinear softening model and double K fracture criterion for quasi-brittle fracture of pultruded FRP composites. Compos Struct 2017;160:1119–25.
[6] Cavaleri L, Di Paola M, Ferrotto MF, Valenza A. Structural performances of pultruded GFRP emergency structures – Part 2: Full-scale experimental testing. Compos Struct 2019;214(15):304–15.
[7] Cavaleri L, Di Paola M, Ferrotto MF, Scalici T, Valenza A. Structural performances of pultruded GFRP emergency structures - Part 1: Experimental characterization of materials and substructure. Compos Struct 2019;214(15):325–34.
[8] National Research Council of Italy. Guide for the design and construction of structures made of FRP pultruded elements, CNR DT 205, Rome; October 2008.
[9] Ascione L et al. Prospect for new guidance in the design of FRP. JRC science and policy report, JRC99714, EUR 27666 EN European Union, Luxembourg, ISBN 978-92-79-54225-1.
[10] China Association for Engineering Construction Standardization. Technical specification for structure of pultruded fiber reinforced polymer composites. T/CECS 692-2020; 2020.
[11] ASCE. Pre-standard for load & resistance factor design (LRFD) of pultruded fiber reinforced polymer (FRP) structures. Reston, VA; 2010.
[12] Bank LC, Mosallam AS, McCoy GT. Design and performance of connections for pultruded frame structures. J Reinf Plast Compos 1994;13(3):199–212.
[13] Bank LC, Yin J, Moore L, Evans DJ, Allison RW. Experimental and numerical evaluation of beam-to-column connections for pultruded structures. J Reinf Plast Compos 1996;15(10):1052–67.
[14] Smith SJ, Parsons ID, Hjelmstad KD. An experimental study of the behavior of connections for pultruded GFRP I-beams and rectangular tubes. Compos Struct 1998;42(3):281–90.
[15] Carrion JE, LaFave JM, Hjelmstad KD. Experimental behavior of monolithic composite cuff connections for fiber reinforced plastic box sections. Compos Struct 2005;67(3):333–45.
[16] Singamsethi SK, LaFave JM, Hjelmstad KD. Fabrication and testing of cuff connections for GFRP box sections. J Compos Constr 2005. https://doi.org/10.1061/(ASCE)1090-0268(2005)9:6(536).
[17] Qiu C, Feng P, Yang Y, Zhu L, Bai Y. Joint capacity of bonded sleeve connections for tubular fibre reinforced polymer members. Compos Struct 2017;163:267–79.
[18] Qureshi J, Mottram JT. Response of beam-to-column web cleated joints for FRP pultruded members. J Compos Constr 2013. https://doi.org/10.1061/(ASCE)CC.1943-5614.0000392.
[19] Sadowski T, Golewski P, Zarzeka-Raczkowska E. Damage and failure processes of hybrid joints: adhesive bonded aluminium plates reinforced by rivets. Comput Mater Sci 2011;50(4):1256–62.
[20] Sadowski T, Kneć M, Golewski P. Experimental investigations and numerical modelling of steel adhesive joints reinforced by rivets. Int J Adhes Adhes 2010;30(5):338–46.
[21] Kelly G. Load transfer in hybrid (bonded/bolted) composite single-lap joints. Compos Struct 2005;69(1):35–43.
[22] Hizam RM, Manalo AC, Karunasena W, Bai Y. Behaviour of pultruded GFRP truss system connected using through-bolt with mechanical insert. Compos B: Eng 2019;168:44–57.
[23] Lee YH, Lim DW, Choi JH, Kweon JH, Yoon MK. Failure load evaluation and prediction of hybrid composite double lap joints. Compos Struct 2010;92(12):2916–26.
[24] Fu M, Mallick PK. Fatigue of hybrid (adhesive/bolted) joints in SRIM composites. Int J Adhes Adhes 2001;21(2):145–59.
[25] Hai ND, Mutsuyoshi H. Structural behavior of double-lap joints of steel splice plates bolted/bonded to pultruded hybrid CFRP/GFRP laminates. Constr Build Mater 2012;30:347–59.
[26] Park HJ. Bearing failure analysis of mechanically fastened joints in composite laminates. Compos Struct 2001;53(2):199–211.
[27] Kim KS, Yoo JS, Yi YM, Kim CG. Failure mode and strength of uni-directional composite single lap bonded joints with different bonding methods. Compos Struct 2006;72(4):477–85.
[28] Razaqpur AG, Ascione F, Lamberti M, Spadea S, Malagic M. GFRP hollow column to built-up beam adhesive connection: mechanical behaviour under quasi-static, cyclic and fatigue loading. Compos Struct 2019;224:111069.
[29] Kelly G. Quasi-static strength and fatigue life of hybrid (bonded/bolted) composite single-lap joints. Compos Struct 2006;72(1):119–29.
[30] Barut A, Madenci E. Analysis of bolted–bonded composite single-lap joints under combined in-plane and transverse loading. Compos Struct 2009;88(4):579–94.
[31] Bois C, Wargnier H, Wahl JC, Le Goff E. An analytical model for the strength prediction of hybrid (bolted/bonded) composite joints. Compos Struct 2013;97:252–60.
[32] Paroissien E, Lachaud F, Schwartz S, Da Veiga A, Barrière P. Simplified stress analysis of hybrid (bolted/bonded) joints. Int J Adhes Adhes 2017;77:183–97.
[33] Feng P, Cheng S, Bai Y, Ye L. Mechanical behavior of concrete-filled square steel tube with FRP-confined concrete core subjected to axial compression. Compos Struct 2015;123:312–24.
[34] Ministry of Housing and Urban-Rural Development of the People's Republic of China (MOHURD). Specification for seismic test of buildings. JGJ 101. Beijing; 2015 (in Chinese).

[35] Applied Technology Council (ATC). Guidelines for seismic testing of components of steel structures. Rep. No. 24, ATC, Redwood City, CA; 1992.
[36] Feroldi F, Russo S. Mechanical performance of pultruded FRP plates in beam-to-beam connections. J Compos Constr 2017;21(4):04017004.
[37] Russo S. Buckling interactions in columns made by built-up thin, open, pultruded FRP shapes. J Reinf Plast Compos 2015;34:972–88.
[38] Russo S. A review on buckling collapses of simple and complex columns made from pultruded FRP material. Compos: Mech Computat Appl Int J 2017;8(1):1–34.
[39] Noh J, Ghadimi B, Russo S, Rosano M. Assessment of FRP pultruded elements under static and dynamic loads. Compos Struct 2018;202:17–28.
[40] Liu T, Vieira JD, Harries KA. Predicting flange local buckling capacity of pultruded GFRP I-sections subject to flexure. J Compos Constr 2020;24(4):04020025.
[41] Liu T, Harries KA. Flange local buckling of pultruded GFRP box beams. Compos Struct 2018;189:463–72.
[42] Liu T, Feng P, Wu Y, Liao S, Meng X. Developing an innovative curved-pultruded large-scale GFRP arch beam. Compos Struct 2021;256:113111.
[43] Rodrigues H, Varum H, Arêde A, Costa A. A comparative analysis of energy dissipation and equivalent viscous damping of RC columns subjected to uniaxial and biaxial loading. Eng Struct 2012;35(Feb):149–64.
[44] Otani S. Hysteresis models of reinforced concrete for earthquake response analysis. J Faculty Eng Univ Tokyo Series A 1981;XXXVI(2):407–41.
[45] Simulia DS. Abaqus 6.14 documentation. Providence, Rhode Island, US; 2014.
[46] Feroldi F, Russo S. Structural behavior of all-FRP beam-column plate-bolted joints. J Compos Constr 2016. https://doi.org/10.1061/(ASCE)CC.1943-5614.0000667.
[47] Russo S. First investigation on mixed cracks and failure modes in multi-bolted FRP plates. Compos Struct 2016;154:17–30.